7060 *Biochemistry* **2010,** *49,* 7060–7068
DOI: 10.1021/bi100866b

BIOCHEMISTRY
including biophysical chemistry & molecular biology
Article

Identification of a Hemerythrin-like Domain in a P_{1B}-Type Transport ATPase[†]

Matthew E. Traverso,[‡,§] Poorna Subramanian,[∥] Roman Davydov,[§] Brian M. Hoffman,[‡,§] Timothy L. Stemmler,[∥] and Amy C. Rosenzweig*[,‡,§]

[‡]*Departments of Biochemistry, Molecular Biology, and Cell Biology, and* [§]*Department of Chemistry, Northwestern University, Evanston Illinois 60208, and* [∥]*Department of Biochemistry and Molecular Biology, Wayne State University School of Medicine, Detroit, Michigan 48202*

Received May 28, 2010; Revised Manuscript Received July 22, 2010

ABSTRACT: The P_{1B}-type ATPases couple the energy of ATP hydrolysis to metal ion translocation across cell membranes. Important for prokaryotic metal resistance and essential metal distribution in eukaryotes, P_{1B}-ATPases are divided into subclasses on the basis of their metal substrate specificities. Sequence analysis of putative P_{1B-5}-ATPases, for which the substrate has not been identified, led to the discovery of a C-terminal soluble domain homologous to hemerythrin (Hr) proteins and domains. The Hr domain from the *Acidothermus cellulolyticus* P_{1B-5}-ATPase was cloned, expressed, and purified (P_{1B-5}-Hr). P_{1B-5}-Hr binds two iron ions per monomer and adopts a predominantly helical fold. Optical absorption features of the iron-loaded and azide-treated protein are consistent with features observed for other Hr proteins. Autoxidation to the met form is very rapid, as reported for other prokaryotic Hr domains. The presence of a diiron center was confirmed by electron paramagnetic resonance (EPR) and X-ray absorption spectroscopic (XAS) data. The occurrence of a Hr-like domain in a P-type ATPase is unprecedented and suggests new regulatory mechanisms as well as an expanded function for Hr proteins in biology.

The P-type ATPases are a large family of integral membrane proteins that couple the energy of ATP hydrolysis to the transport of cations across cell membranes (*1*). Named for the formation of a phosphorylated intermediate during catalysis, P-type ATPases are classified on the basis of their substrate specificities and include the Ca^{2+}-, Na^+/K^+-, and H^+-ATPases (*2*). Members of the P_{1B} subgroup transport transition metal ions, including $Zn^{2+}/Cd^{2+}/Pb^{2+}$ (*3*−*5*), Cu^{2+} (*6*), Cu^+/Ag^+ (*7*), and Co^{2+} (*8*). Widely distributed in nature, the P_{1B}-ATPases confer heavy metal tolerance to microorganisms (*9*) and are essential for the absorption, distribution, and bioaccumulation of metal micronutrients by cyanobacteria (*10*) and eukaryotes (*11*, *12*). In humans, mutations in the Cu^+ ATPases ATP7A and ATP7B lead to Menkes syndrome and Wilson disease, respectively (*13*).

All P_{1B}-ATPases have the same core architecture consisting of at least six transmembrane (TM)[1] helices, a soluble ATP binding domain (ATPBD), and a soluble actuator domain (A-domain), both located in the cytoplasm (Figure 1). The ATPBD includes the nucleotide binding site and a conserved DKTGT motif, of which the aspartic acid residue is phosphorylated in the catalytic cycle. Residues in the last three TM helices are proposed to form the metal binding site(s), and specificity is proposed to derive from the identities and positions of coordinating residues within these helices (*14*, *15*). In particular, a three-residue cysteine-containing sequence motif in TM helix 4 or 6 is important for metal transport activity (*16*, *17*). On the basis of sequence analysis and experimental evidence, the P_{1B}-ATPases have been further divided into five substrate-specific subfamilies, designated P_{1B-1} through P_{1B-5} (*14*, *15*).

Most P_{1B}-ATPases include two additional TM helices as well as one or more soluble cytoplasmic metal binding domains (MBDs) at the N- and/or C-termini. Many MBDs from P_{1B-1}- and P_{1B-2}-ATPases exhibit a conserved ferredoxin-like fold and bind metal ions via conserved CXXC sequence motifs (*18*). Other types of histidine- and cysteine-rich MBDs found in the P_{1B-3}- and some P_{1B-2}-ATPases have also been shown to bind metal ions (*19*). A large body of data indicates that the MBDs play a regulatory role in ATPase function (*19*, *20*). The P_{1B-4}- and P_{1B-5}-ATPases are the least well characterized and are distinguished by their relatively simple architecture, including only six TM helices (Figure 1) and an apparent absence of soluble MBDs (*15*). Whereas the P_{1B-4}-ATPases are associated with transport of Co^{2+} and other divalent metal ions (*8*, *21*), the substrate for the P_{1B-5}-ATPases has not yet been identified.

Here we report the identification, isolation, and characterization of a soluble domain found at the C-terminus of P_{1B-5}-ATPases. Surprisingly, this domain is homologous to hemerythrins (Hr), a family of proteins and domains characterized by the presence of a carboxylate-bridged diiron center housed within a four-helix bundle (*22*). Characterization of this Hr-like domain from the P_{1B-5}-ATPase of *Acidothermus cellulolyticus*, a Gram-positive cellulolytic thermophile, reveals the presence of a diiron center. The presence of a Hr-like domain in a P_{1B}-ATPase is unprecedented and provides insight into P_{1B-5}-ATPase function and the role of Hr proteins in biology.

MATERIALS AND METHODS

Bioinformatic Analysis and Sequence Alignments. Five P_{1B-5}-ATPase sequences identified previously (*14*) were used as

[†]This work was supported by NIH Grants GM58518 (A.C.R.), DK068139 (T.L.S.), and HL13531 (B.M.H).

*Corresponding author. Tel: 847-467-5301. Fax: 847-467-6489. E-mail: amyr@northwestern.edu.

[1]Abbreviations: A-domain, actuator domain of a P_{1B}-type ATPase; ATPBD, ATP binding domain of a P_{1B}-type ATPase; DcrH-Hr, hemerythrin domain from *Desulfovibrio vulgaris* chemotaxis protein; EPR, electron paramagnetic resonance; EXAFS, extended X-ray absorption fine structure; Hr, hemerythrin; MBD, metal binding domain; P_{1B-5}-Hr, hemerythrin domain from the *Acidothermus cellulolyticus* P_{1B-5}-ATPase; TM, transmembrane; XANES, X-ray absorption near edge spectra.

 Published on Web 07/23/2010

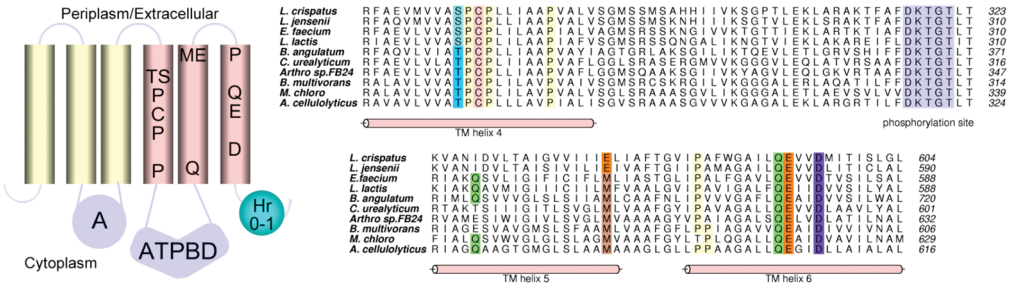

FIGURE 1: Architecture and sequences of P_{1B-5}-ATPases. Left: Overall topology, including a novel Hr-like C-terminal soluble domain. Conserved residues in TM helices are shown in approximate locations. Right: Noncontinuous alignments of TM helix 4 and the start of the ATPBD (top) and TM helices 5 and 6 (bottom) of ten representative P_{1B-5}-ATPases. Generally conserved residues that may play a role in substrate specificity are colored with cysteine in pink, proline in yellow, serine in cyan, threonine in blue, glutamine in green, aspartate in violet, glutamate in orange, and methionine in brown. The phosphorylation site in the ATPBD is highlighted in lavender. The helices below the sequences indicate putative TM helices. The sequences correspond to the following proteins: *L. crispatus*, GI 256849544, UnitProtKB C7Y4W5; *L. jensenii*, GI 260665179, UniProtKB D0DPP6; *E. faecium*, GI 69245746, UniProtKB C9CF69; *L. lactis*, GI 15672077, UniProtKB Q9CJA5; *B. angulatum*, GI 229816919, UniProtKB C4FCZ1; *C. urealyticum*, GI 172040330, UniProtKB B1VFS1; *Arthrobacter* sp. FB24, GI 116668908, UniProtKB A0JRS1; *B. multivorans*, GI 161522885, UniProtKB A9ASK0; *M. chloromethanicum*, GI 218529299, UniProtKB B7KQY2; *A. cellulolyticus*, GI 117927237, UniProtKB A0LQU2.

an initial query using protein−protein PSI-BLAST (*23*) (blastp) searches against the NCBI database. Both InterPro (*24*) and Pfam (*25*) analyses of many of the sequences indicated the presence of a C-terminal Hr/HHE (histidine−histidine−glutamate) cation binding domain (PF01814, IPR012312). Sections of the *Streptomyces coelicolor* P_{1B-5}-ATPase sequence (UniProtKB Q9RJ01), including the fourth TM helix and the start of the ATPBD as well as the C-terminal Hr domain, were then used for further queries. Sequences were aligned by the ClustalW method (*26*) with manual adjustments to ensure the best possible alignment of conserved metal binding residues. Secondary structure predictions were performed using the SOPMA secondary structure prediction method (*27*). The TopPred server (*28*) was used to predict the number and location of TM helices, and SignalP 3.0 (*29*) was used to identify signal peptide cleavage sites

Cloning and Expression of a P_{1B-5}-ATPase Hr Domain. The gene sequence encoding the C-terminal domain (residues 620−775) of the *A. cellulolyticus* 11B (*30*) P_{1B-5}-ATPase (YP_871788) was PCR amplified from genomic DNA (ATCC) with PCR master mix (Fermentas) using the primers 5′-CTGGTCGGTCTCGAATGCTGCCGGGTACGCGACAC-3′ and 5′-CTGGTCGGTCTCGGCGCTGCGCTGACCGGCATCCGGTAG-3′ (IDT), which introduce *Bsa*I restriction sites. This sequence was selected by aligning the amino acid sequence of *A. cellulolyticus* P_{1B-5}-ATPase with that of DcrH-Hr (Figure 2), the C-terminal domain of a *Desulfovibrio vulgaris* chemotaxis protein, and the best characterized prokaryotic Hr domain (*31*). The homologous region begins at Leu 620 and continues to Arg 775 but does not include the final 19 amino acids of the P_{1B-5}-ATPase. Secondary structure predictions suggest that these final residues are random coil whereas the rest of the sequence is predicted to be helical, as is characteristic of Hr domains (*22*, *32*).

The purified PCR product and the plasmid pPR-IBA1 (IBA) were digested with *Bsa*I (New England Biolabs), purified, and ligated, creating a construct containing an eight-residue streptactin tag with a two-residue linker (SAWSHPQFEK) fused to the C-terminus of the protein. The vector was transformed into *E. cloni* 10G chemically competent cells (Lucigen) following the manufacturer's protocol and spread on a Luria−Bertani (LB) plate containing 100 μg/mL ampicillin. DNA sequencing of individual colonies confirmed the presence and accuracy of the gene fragment encoding the Hr-like domain, designated P_{1B-5}-Hr.

For protein expression, BL21(DE3) *Escherichia coli* chemically competent cells were transformed with the plasmid encoding P_{1B-5}-Hr. Baffled flasks containing 1 L LB media supplemented with 100 mg of ampicillin were inoculated with an overnight culture of cells and grown at 37 °C with shaking. Protein expression was induced by adding 1 mM IPTG at an OD_{600} of approximately 0.6. Cells continued to grow for an additional 3−4 h, after which they were harvested by centrifugation at 4800*g* for 10 min in a Sorvall SLC 4000 rotor at 4 °C and stored at −80 °C.

Protein Purification. All purification and handling steps were conducted at 4 °C. The cells were resuspended in a buffer containing 50 mM Tris, pH 7.0, 200 mM NaCl, and 0.5 mM PMSF and lysed by sonication for 8 min by using 20 s pulses with a 40 s rest period between each pulse. Insoluble cell debris was removed by ultracentrifugation at 120000*g* in a Beckman TI-60 rotor for 1 h. The supernatant was loaded onto streptactin resin (Qiagen) and washed with four column volumes of a 50 mM Tris, pH 7.0, 200 mM NaCl wash buffer. The protein was then eluted with 1.5 column volumes of wash buffer supplemented with 2.5 mM desthiobiotin. The eluted sample (as-isolated P_{1B-5}-Hr) was concentrated in an Amicon 15 mL spin concentrator with a 10 kDa filter, and its concentration was measured by the Lowry assay (*33*) using bovine serum albumin as a standard.

Metal Loading and Analysis. The metal content was measured by inductively coupled plasma optical emission spectrometry (ICP-OES) using a Varian Vista MPX ICP-OES in the Integrated Molecular Structure Education and Research Center (IMSERC) at Northwestern University. As-isolated samples were digested in 5 mL of 5% Trace SELECT nitric acid (Sigma Aldrich) in chelexed water and then filtered if necessary. Standards of iron, chromium, nickel, cobalt, zinc, copper, molybdenum, manganese, vanadium, and cadmium (Sigma Aldrich) were prepared in 5% nitric acid as well. Iron loading was performed by the aerobic addition of 2 equiv of $Fe(NH_4)_2(SO_4)_2 \cdot 6H_2O$ in 100 mM MES acid, pH 3.0, and 200 mM ascorbic acid to the protein solution followed by gentle mixing for 30 min. The protein was then exchanged into a buffer containing 25 mM Tris, pH 7.0, and 100 mM NaCl using a 10DG desalting column (Bio-Rad). The protein and metal concentrations were measured by the Lowry assay and ICP-OES, respectively. To test whether P_{1B-5}-Hr binds metals other than iron, an apo sample was prepared by adding 10 mol equiv of desferrioxamine (Sigma Aldrich) followed by desalting. Five equivalents of different metal ions ($MnCl_2$,

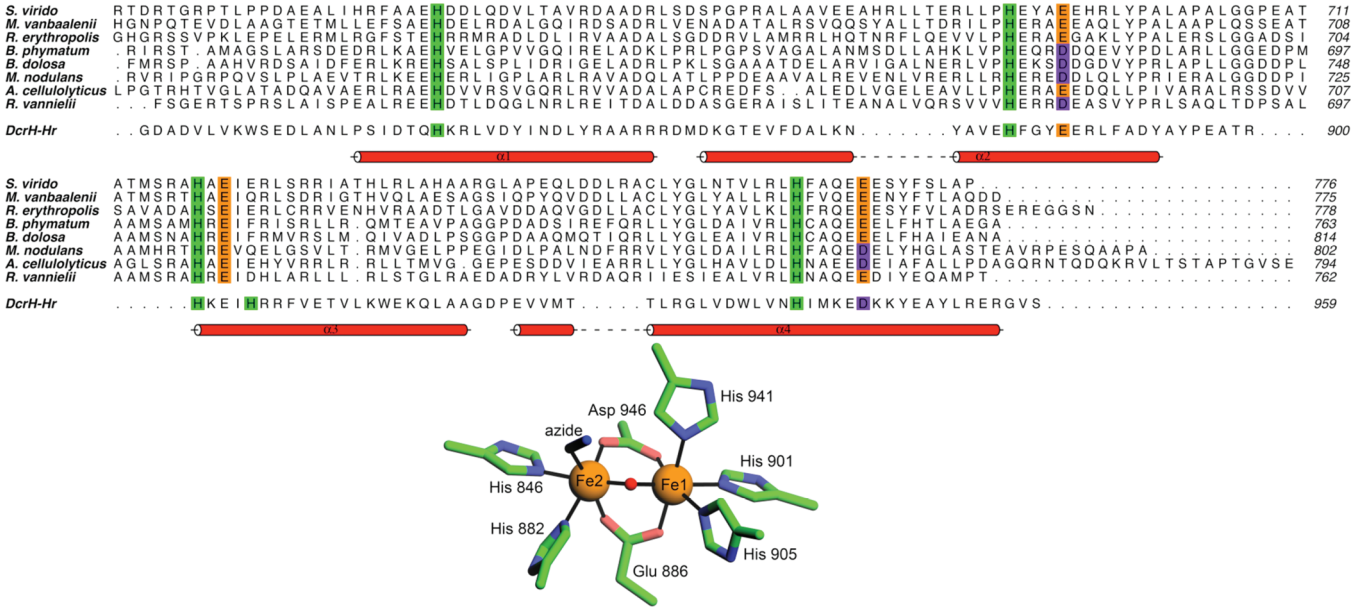

FIGURE 2: The hemerythrin domain of P_{1B-5}-ATPases. Top: Alignment of eight representative P_{1B-5}-Hr sequences with the Hr domain of DcrH (DcrH-Hr, GI 887858, UniProtKB Q46583). The metal-binding residues of DcrH-Hr along with corresponding residues from P_{1B-5}-Hrs are colored with histidine in green, glutamic acid in orange, and aspartic acid in violet. The red helices below the sequence correspond to the known secondary structure elements of DcrH-Hr. The P_{1B-5}-Hr sequences correspond to the following proteins: *S. viridochromogenes*, GI 256799641; *M. vanbaalenii*, GI 120402396, UniProtKB A1T4W9; *R. erythropolis*, GI 226306903, UniProtKB C1A0I9; *B. phymatum*, GI 186471018, UniProtKB B2JWG3; *B. dolosa*, GI 254255483, UniProtKB A2WJ24; *M. nodulans*, GI 220919964, UniProtKB B8IWI5; *A. cellulolyticus*, GI 117927237, UniProtKB A0LQU2; *R. vannielii*, GI 283824493, UniProtKB D2LJH3. Bottom: The structure of the diiron center in the azide adduct of DcrH-Hr (PDB accession code 2AVK).

$Fe(NH_4)_2(SO_4)_2$, $CoCl_2$, $NiCl_2$, $CuCl_2$, $Zn(OAc)_2$, or $CdCl_2$) were added to this apo P_{1B-5}-Hr, followed by desalting and Lowry and ICP-OES analysis.

Analytical Gel Filtration Chromatography. Analytical gel filtration chromatography was performed on a 22.5 mL Superdex 75 (GE Healthcare) column equilibrated with 50 mM Tris, pH 7.0, and 200 mM NaCl. Two hundred microliters of either as-isolated or iron-loaded P_{1B-5}-Hr was loaded onto the column, and molecular masses were determined using the following standards: blue dextran (void volume); aldolase, 158 kDa; ovalbumin, 43 kDa; chymotrypsin, 25 kDa; and RNase A, 13.7 kDa.

Optical and Circular Dichroism Spectroscopy. All spectra were collected at room temperature. The UV−visible spectra of P_{1B-5}-Hr (500 μM) were recorded using a Perkin-Elmer LAMBDA 1050 spectrophotometer. The azide adduct was generated by adding 50 mol equiv of NaN_3 per diiron center and incubating for 20−30 min prior to spectroscopic measurements. Reduced and oxidized samples were obtained by adding 10 mol equiv of NaS_2O_4 and 1 mol equiv of $K_3Fe(CN)_6$ per diiron center, respectively, and gently mixing immediately before spectroscopic measurements. Circular dichroism (CD) spectra were recorded on a JASCO J-815 spectrometer using a 0.6 mm path length quartz cuvette and protein diluted to 100 μM concentration in 50 mM Tris, pH 7.0, and 200 mM NaCl. An average of three scans was collected at 20 °C with 1 nm resolution.

Thermal Stability Assay. Apo and iron-loaded P_{1B-5}-Hr were concentrated to 2−5 mg/mL and mixed with thermal stability buffer (100 mM HEPES, pH 7.5, 150 mM NaCl) and 5000× SYPRO Orange (Molecular Probes, Inc.) in DMSO in a 25:120:2 ratio. One microliter of each solution was distributed into each well of a PCR plate. The wells were then filled with 10 μL of buffer containing 50 mM Tris, pH 7.0, and 200 mM NaCl with some wells containing 5 mg/mL desferrioxamine as well. The plates were sealed and transferred to a Bio-Rad CFX384 real-time PCR detection system in the High Throughput Analysis Laboratory at Northwestern University. The temperature of the plates was increased at a rate of 0.5 °C per minute over the range of 10−95 °C, and fluorescence was monitored at 570 nm. The data were processed using OriginPro 6.1 for Windows. In order to determine the inflection point of the melting curves, which was assumed to equal the melting temperature (T_m), a Boltzmann sigmoidal equation was fitted to the raw data. This experiment was performed in replicate up to 20 times to ensure T_m precision.

Electron Paramagnetic Resonance (EPR) Spectroscopy. Samples for EPR were concentrated to 1 mM protein in 25 mM Tris, pH 7.0, 100 mM NaCl, and 20% glycerol, transferred to Q-band EPR tubes, frozen, and stored in liquid nitrogen. Cryoreduction and signal quantitation were carried out as described previously (*34*). Annealing at 260 K was performed by placing the EPR sample in a salt water bath and then freezing in liquid nitrogen (*35*). X-band spectra were collected at 10 K using a Bruker ESP300 spectrometer with the field modulation set to 10 G.

X-ray Absorption Spectroscopy. For X-ray absorption spectroscopy (XAS), samples were prepared in 25 mM Tris, pH 7.0, 100 mM NaCl, and 30% glycerol with iron concentrations in the 1−2 mM range. Two independent replicates of iron-loaded P_{1B-5}-Hr and P_{1B-5}-Hr in the presence of 50 mol equiv of NaN_3 were prepared. Samples were loaded into Lucite cells wrapped with Kapton tape and frozen in liquid nitrogen. XAS data were collected at the Stanford Synchrotron Radiation Lightsource (SSRL) on beamline 7-3, equipped with a single rhodium-coated silicon mirror and a Si[220] double crystal monochromator detuned 50% for harmonic rejection. Samples were maintained at 10 K using an Oxford Instruments continuous-flow liquid helium cryostat. Protein fluorescence excitation spectra were collected using a 30-element Ge solid-state array detector. XAS spectra were measured as described previously (*36*). Data were processed

Table 1: Summary of Raw Fe EXAFS Simulation Analysis for Iron-Loaded and Azide-Treated *A. cellulolyticus* P_{1B-5}-Hr[a]

		Fe−nearest-neighbor ligands[b]				Fe−long-range ligands[b]				
sample	fit no.	atom[c]	R (Å)[d]	CN[e]	σ^2[f]	atom[c]	R (Å)[d]	CN[e]	σ^2[f]	F′[g]
Fe	1	O/N	1.97	2.5	4.7	C	3.03	1.0	2.6	0.30
		O/N	2.09	2.5	4.6	C	3.46	2.5	1.3	
	2	O/N	1.97	2.5	4.91	C	3.02	1.0	5.5	0.27
		O/N	2.10	2.5	5.3	Fe	3.39	1.0	4.8	
	3	**O/N**	**1.97**	**2.5**	**4.9**	**C**	**3.02**	**1.0**	**5.7**	**0.25**
		O/N	**2.10**	**2.5**	**5.4**	**Fe**	**3.39**	**1.0**	**4.7**	
						C	**4.09**	**1.0**	**4.9**	
azide	1	O/N	1.99	2.5	4.3	C	3.04	1.0	2.0	0.21
		O/N	2.12	2.5	4.1	C	3.46	3.5	2.8	
	2	O/N	1.99	2.5	5.0	C	3.03	1.0	3.5	0.16
		O/N	2.11	2.5	5.8	Fe	3.39	1.0	4.3	
	3	**O/N**	**1.99**	**2.5**	**5.0**	**C**	**3.03**	**1.0**	**3.3**	**0.14**
		O/N	**2.11**	**2.5**	**5.7**	**Fe**	**3.39**	**1.0**	**4.2**	
						C	**4.12**	**1.0**	**3.0**	

[a]Values given in bold represent the best-fit simulation parameters. [b]Independent metal−ligand scattering environment. [c]Scattering atoms: O (oxygen), N (nitrogen), C (carbon), and Fe (iron). [d]Metal−ligand bond length (all standard deviations < 0.03 Å). [e]Metal−ligand coordination number (all standard deviations < 1.0). [f]Debye−Waller factor given in $Å^2 \times 10^3$ (all standard deviations < 0.9 Å). [g]Number of degrees of freedom weighted mean square deviation between empirical and theoretical data.

using the Macintosh OS X version of the EXAFSPAK program suite integrated with the Feff v7.2 software for theoretical model generation. XAS data reduction and analysis were performed following previously reported protocols (*37*). EXAFS data were simulated over a k range of 1−14.2 $Å^{-1}$ for a spectral resolution of 0.12 Å. Data were fit using a scale factor of 0.95 and E_o values for Fe−O/N/C and Fe−Fe interactions of −10 and −15, respectively. Simulation parameters for fitting the raw unfiltered data are given along with the number of degrees of freedom weighted simulation "goodness of fit" (F') parameter in Table 1.

RESULTS AND DISCUSSION

Sequence Characteristics of Hr Domain-Containing P_{1B-5}-ATPases. A BLAST search using a 60-residue sequence from the *S. coelicolor* P_{1B-5}-ATPase, one of the previously identified P_{1B-5}-ATPases (*14*), corresponding to the fourth TM helix and the start of the ATPBD yielded 195 complete P_{1B-5}-ATPase sequences. This residue span was selected because it includes residues in the putative TM metal binding site proposed to confer substrate specificity, including the cysteine- and proline-containing signature motif. It is therefore ideal for distinguishing members of the P_{1B-5}-ATPase subfamily. Every species containing a P_{1B-5}-ATPase is eubacterial, but beyond this broad classification, there are no obvious unifying characteristics. P_{1B-5}-ATPases are found in Gram-positive, Gram-negative, aerobic, anaerobic, facultative, and microaerobic organisms. Of the 195 identified sequences, 40 contained Hr-like domains. Membrane topology predictions indicate the presence of six to seven TM helices. Those proteins that have seven predicted TM helices, including the *A. cellulolyticus* P_{1B-5}-ATPase, contain a signal peptide cleavage site between the first two helices, consistent with a six-helix architecture. The P_{1B-4}-ATPases are also predicted to have six TM helices, and these six helices correspond to the final six helices of the eight helix P_{1B-1}-, P_{1B-2}-, and P_{1B-3}-ATPases (*15*).

With a larger library of sequences identified, the defining characteristics of the P_{1B-5} subfamily (*14*) can be refined (Figure 1). Alignment of the 195 P_{1B-5}-ATPase sequences (Supporting Information Figure S1) indicates that the signature sequence in the fourth TM helix is (T/S)PCP with threonine present in 113 sequences and serine in the other 82 sequences. In 143 of 195 sequences, the fifth TM helix begins with a glutamine. The fifth helix also contains a conserved potential metal binding residue near the periplasmic face, a methionine in 171 sequences and a glutamic acid in 24 sequences. The final TM helix houses a QEXXD motif that is conserved in all but two P_{1B-5}-ATPases. This motif along with the (T/S)PCP sequence likely contributes key substrate binding residues. Previously noted serine and asparagine residues in the fifth and sixth helices, respectively (*14*), are not universally conserved in this more extensive sequence library.

Like most P_{1B-4}-ATPases, the P_{1B-5}-ATPases lack N-terminal soluble MBDs, suggesting that the two N-terminal TM helices in the other subfamilies may serve to tether and position the MBDs for regulatory interactions with the other soluble domains. The only exception, from *Burkholderia glumae*, contains a membrane-bound cytochrome b_{561}-like domain (PF01292, IP011577) fused to the N-terminus. The P_{1B-5}-ATPases are common to the *Burkholderia* genus, and a gene encoding a cytochrome b_{561}-like protein is sometimes found in the same operon (e.g., *Burkholderia cenocepacia* J2315, *Burkholderia vietnamiensis* G4, *Burkholderia ambifaria* MC40-6, *Burkholderia multivorans* ATCC 17616). In some organisms, these cytochrome b_{561} proteins are associated with NiFe hydrogenases (*38*, *39*), although this enzyme does not appear to be present in all *Burkholderia* genomes encoding a P_{1B-5}-ATPase.

The only C-terminal soluble domain found in the P_{1B-5}-ATPases is the Hr-like domain. Interestingly, all 40 Hr-containing P_{1B-5}-ATPases have the conserved methionine in the fifth TM helix, and 38 have a TPCP signature motif in the fourth helix. These Hr domains were not identified in recent studies of Hr diversity and classification (*40*, *41*), probably due to the low overall sequence homology. For example, *A. cellulolyticus* P_{1B-5}-Hr is 18% identical and 40% similar to DcrH-Hr. Moreover, the metal binding residues are not completely conserved. In structurally characterized eukaryotic and prokaryotic Hr proteins, the two iron ions are bridged by an aspartic acid and a glutamic acid and coordinated by three and two histidines, respectively (*22*, *32*) (shown for DcrH-Hr in Figure 2). In 27 of 40 sequences, the residue corresponding to DcrH-Hr Asp 946 (numbering based on the full-length DcrH sequence) is glutamic acid, and in 23 sequences, aspartic acid replaces DcrH-Hr Glu 886. Moreover, one of the metal coordinating histidine residues, equivalent to DcrH-Hr His 905, is completely absent in all of the P_{1B-5}-ATPase Hr domains (Figure 2). Some of the identified P_{1B-5}-Hr sequences have a histidine one amino acid later, yielding HX_4H rather than HX_3H, but this only occurs in 7 of the 40 sequences, suggesting it may not be involved in metal binding. There is a conserved glutamic acid two amino acids prior to the histidine position. Thus, the consensus motif of P_{1B-5}-Hr is H-HX_3(D/E)-HXE-HX_4(E/D). In *A. cellulolyticus* P_{1B-5}-Hr, these residues are His 644, His 685, Glu 689, His 714, Glu 716, His 757, and Asp 762. Alterations in the metal binding residues are found in a large number of predicted prokaryotic Hrs (*41*). In addition, there are significant deviations between the hydrophobic substrate channel residues of classical Hr domains and the corresponding residues in the P_{1B-5}-Hr proteins. Of the 21 residues that comprise the substrate channel in DcrH-Hr (*32*), only seven are similar in P_{1B-5}-Hr proteins.

Isolation and Characterization of P_{1B-5}-Hr. Overexpression of P_{1B-5}-Hr yielded approximately 3 mg of purified protein/1 L of media. The single-step purification on the streptactin column was sufficient for $> 95\%$ purity (Figure 3). Samples were analyzed

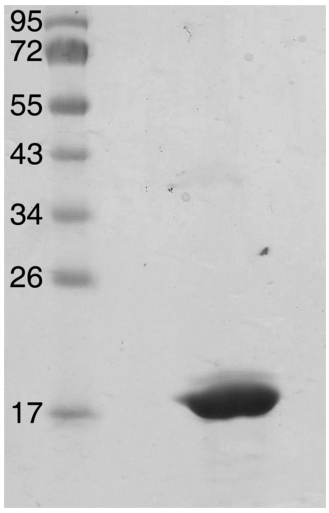

FIGURE 3: SDS−PAGE analysis of purified *A. cellulolyticus* P_{1B-5}-Hr. Molecular mass markers are labeled in kDa. The predicted molecular mass of *A. cellulolyticus* P_{1B-5}-Hr is 18.5 kDa.

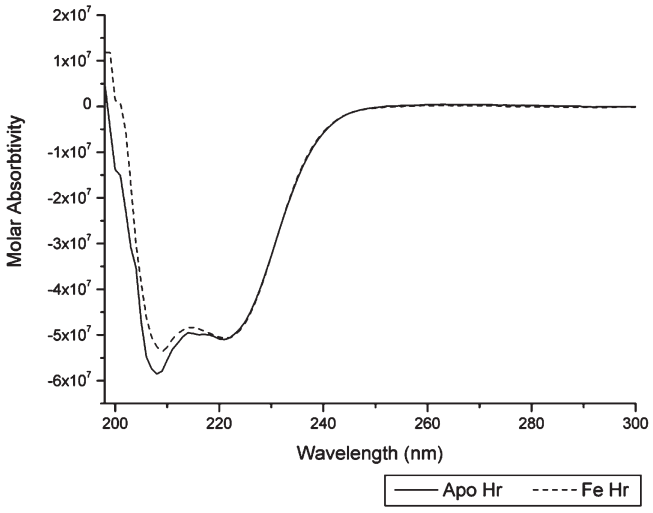

FIGURE 4: CD spectrum of apo and iron-loaded *A. cellulolyticus* P_{1B-5}-Hr (150−200 μM) in 50 mM Tris, pH 7.0, and 200 mM NaCl.

for a range of metal ions by ICP-OES, and only iron was detected. The iron stoichiometry was variable, with values ranging from 0 to 2 iron ions per protein monomer. If the stoichiometry was less than 2 iron ions per protein, 2 equiv of $Fe(NH_4)_2(SO_4)_2 \cdot 6H_2O$ was added, and then excess iron was removed on a desalting column. After this treatment, the stoichiometry was 2.13 ± 0.10 iron ions per protein. An apo form of P_{1B-5}-Hr was prepared by desferrioxamine treatment and then loaded with 5 equiv of Mn(II), Fe(II), Co(II), Ni(II), Cu(II), Zn(II), and Cd(II). Stoichiometries of 0.22 ± 0.01 Mn(II), 1.93 ± 0.06 Fe(II), 0.75 ± 0.02 Co(II), 0.48 ± 0.03 Ni(II), 1.10 ± 0.01 Cu(II), 1.25 ± 0.12 Zn(II), and 0.92 ± 0.02 Cd(II) were measured. Given the consistent measurement of 2 Fe per protein and the spectroscopic data (vide infra), it seems likely that P_{1B-5}-Hr binds iron specifically and perhaps binds other metal ions adventitiously.

The oligomeric state of P_{1B-5}-Hr in solution was investigated by analytical gel filtration experiments (Supporting Information Figure S1). The as-isolated sample eluted in two peaks, one at ~34 kDa and a second beyond the calibration range but below the void volume (~200 kDa). The theoretical mass of P_{1B-5}-Hr, including streptactin tag and linker, is 18.5 kDa, consistent with the presence of a dimer and a higher molecular mass oligomer. The same two peaks are observed for the iron-loaded sample, although with slightly altered calculated masses of ~40 and > 300 kDa. In addition, an aggregate peak is present, consistent with some precipitation observed upon iron addition.

CD and Optical Spectroscopy. The CD spectra of both apo and iron-loaded P_{1B-5}-Hr exhibit local minima at 209 and 221 nm (Figure 4), indicative of a primarily helical structure, consistent with a Hr four-helix bundle (*22*). The similarity between the CD spectra of the iron-loaded and apo samples suggests that iron binding does not induce major structural changes. The purified, iron-loaded protein is always yellow in color, and its optical spectrum (Figure 5) lacks a ligand-to-metal charge transfer (LMCT) band observed at 500 nm for the oxy form of Hr, which has a terminally bound hydroperoxide ligand (*31*, *42*, *43*). Reduction by excess dithionite bleached the yellow color, which reappeared upon exposure to air, without forming any detectable absorbance features attributable to the oxy form, indicating that autoxidation to the met form is very rapid ($t_{1/2}$ < 1 min). Rapid autoxidation was also reported for the prokaryotic Hr domain DcrH-Hr (*31*) and Hr from *Methylococcus capsulatus* (Bath) (*42*). A shoulder at approximately 650 nm is a d-d transition from the diiron(III) site (*44*). There is a broad absorbance in the 300−400 nm range attributable to LMCT transitions, but distinct peaks are not observed as in other Hr proteins and domains (*31*, *42*, *44*, *45*). Addition of the oxidizing agent potassium ferricyanide did not produce any new spectroscopic features (data not shown), indicating that the iron-loaded sample contains only Fe(III). The spectrum of the Hr domain from the human FBXL5 protein is similar (*46*). Interestingly, alignments indicate that the histidine residue absent in P_{1B-5}-Hr is also missing in FBXL5. Thus, the broader spectroscopic features in the 300−400 nm range may be due to differences in iron coordination in P_{1B-5}-Hr. Addition of azide produces a new optical feature at 453 nm (Figure 5). Similar features are observed for DcrH-Hr (*31*), *M. capsulatus* (Bath) Hr (*42*), and Hr from marine invertebrates (*44*, *47*).

Thermal Stability Assay. To evaluate the effect of iron loading on P_{1B-5}-Hr stability, thermal stability assays were performed. SYPRO Orange, a dye that fluoresces when interacting with hydrophobic residues and can act as an indicator for denatured protein, was mixed with both apo and iron-loaded P_{1B-5}-Hr. These solutions were gradually heated while the fluorescence was monitored, and the signal was normalized to generate a denaturation curve (Figure 6). Fitting of these curves yields T_m values of 65.5 ± 1.5 °C for apo P_{1B-5}-Hr and 74.9 ± 2.0 °C for iron-loaded P_{1B-5}-Hr. To verify that the increased thermostability is a direct effect of the iron bound to P_{1B-5}-Hr, conditions containing an excess of desferrioxamine were tested for thermal stability. Apoprotein was relatively unaffected by the desferrioxamine with a T_m value of 65.8 ± 0.2 °C. The iron-loaded protein, however, exhibited a decreased T_m to 63.4 ± 0.3 °C, effectively equivalent to the apo sample. The T_m of the apoprotein correlates well with temperature-dependent growth of *A. cellulolyticus*, which has a maximum growth temperature of 65 °C.

EPR Spectroscopy. Iron-loaded P_{1B-5}-Hr is EPR silent, consistent with an antiferromagnetically coupled diiron(III) center. Initial attempts to generate an EPR signal by semireduction with dithionite or reduction followed by semioxidation were unsuccessful, perhaps due to instability of the mixed valence state. Instead, to generate a mixed valence Fe(II)Fe(III) center, a frozen, iron-loaded sample was reduced by γ-irradiation as done previously for Hr (*48*) and other diiron-containing proteins,

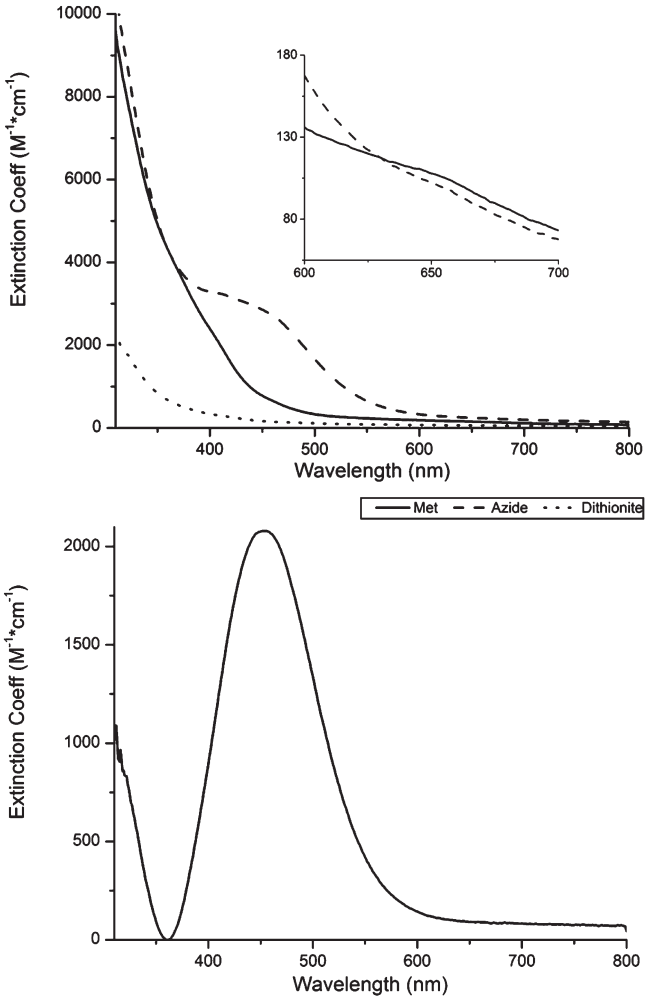

FIGURE 5: Optical spectra of *A. cellulolyticus* P_{1B-5}-Hr. Top: Spectra of iron-loaded, azide-treated, and background-corrected, reduced P_{1B-5}-Hr in 25 mM Tris, pH 7.0, and 100 mM NaCl. The inset shows a shoulder at ~650 nm. The extinction coefficient is reported per diiron center as quantified by ICP OES. Bottom: Difference spectrum generated from the subtraction of the iron-loaded spectrum from the azide absorbance.

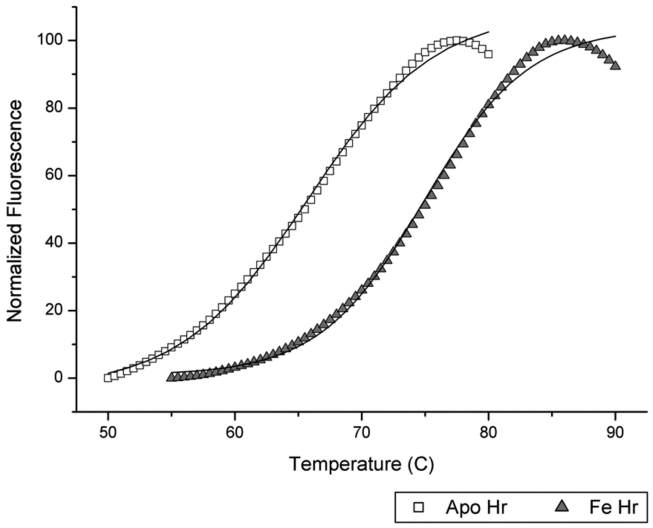

FIGURE 6: Thermal stability fluorescence spectra of apo and iron-loaded P_{1B-5}-Hr with Boltzmann sigmoidal fits. All fluorescence units have been normalized to account for differences in protein concentration.

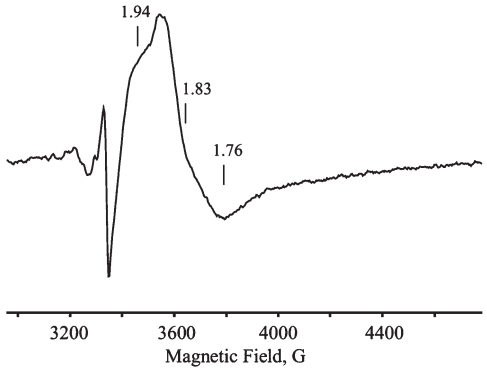

FIGURE 7: X-band EPR spectrum of cryoreduced and annealed iron-loaded *A. cellulolyticus* P_{1B-5}-Hr. The spectrum was collected at 10 K with a microwave power of 2 mW.

including the soluble methane monooxygenase hydroxylase (*34*) and the ribonucleotide reductase R2 protein (*48*). After annealing at 260 K to eliminate radicals in the frozen matrix whose signals partly obscured that of cryoreduced P_{1B-5}-Hr, the spectrum from the protein shown in Figure 7 was obtained. The *g*-values of 1.94, 1.83, and 1.76 rule out an assignment to a mononuclear iron center and, instead, definitively reveal the presence of a mixed valence Fe(II)Fe(III) diiron cluster in which the partner Fe ions are antiferromagnetically coupled to generate an $S = {}^1/_2$ cluster state (*48*, *49*). Quantitation with a Cu(II)-EDTA standard indicates that the dose of 1.4 Mrad created ~0.1−0.15 mM Fe(II)-Fe(III) cluster. Our experience indicates that this dose typically reduces roughly 15% of the diamagnetic parent, leading to an estimated total concentration of diiron centers of ~0.75 mM, which corresponds approximately to ~3/4 occupancy of the sites (sample concentration 1 mM). A signal at $g = 4.3$ was also present, and quantitation indicates that the concentration of adventitious Fe(III) is ~0.1 mM or about 10% of the total iron.

X-ray Absorption Spectroscopy. To confirm the presence of a diiron center, XAS data were collected on samples of iron-loaded P_{1B-5}-Hr and P_{1B-5}-Hr in the presence of azide. The X-ray absorption near edge spectra (XANES) indicate the presence of both Fe(II) and Fe(III) in the protein-bound Fe XANES (Figure 8). Analysis of the first inflection energies for protein-bound Fe compared to Fe(II) and Fe(II) model controls indicates that the iron-loaded sample (inflection energy of 7124.6 eV) has a 50% mixture of Fe(II) and Fe(III) whereas the azide-treated sample (inflection energy of 7123.9 eV) has a 65%/35% mixture of Fe(II)/Fe(III). Immediately following exposure of the iron-loaded sample to the X-ray beam, the resulting metal appears to be a stable equivalent mixture of Fe(II) and Fe(III). The azide-treated sample was highly susceptible to X-ray-influenced metal photoreduction.

The extended X-ray absorption fine structure (EXAFS) data for both protein samples are best fit with multiple shells of interacting ligands (Figure 9, Table 1). There are two O/N ligands at 1.97−1.99 Å, four O/N ligands at 2.09−2.12 Å, consistent with six-coordinate iron (Figure 2), and a highly prevalent scattering Fe−Fe signal in both samples at 3.39 Å. This Fe−Fe distance is identical to the 3.39 Å distance observed crystallographically for met DcrH-Hr and longer than the 3.25 Å distance typical of invertebrate Hr (*22*, *50*). An increase in Fe−Fe distance is consistent with the presence of a partly photoreduced diiron center (*32*, *51*). The two nearest-neighbor O/N ligand environments likely correspond to histidine nitrogen atoms and carboxylate oxygen atoms at ~2.1 Å, as observed in other Hr structures, and perhaps exogenous oxygen-based ligands at 1.97−1.99 Å. The

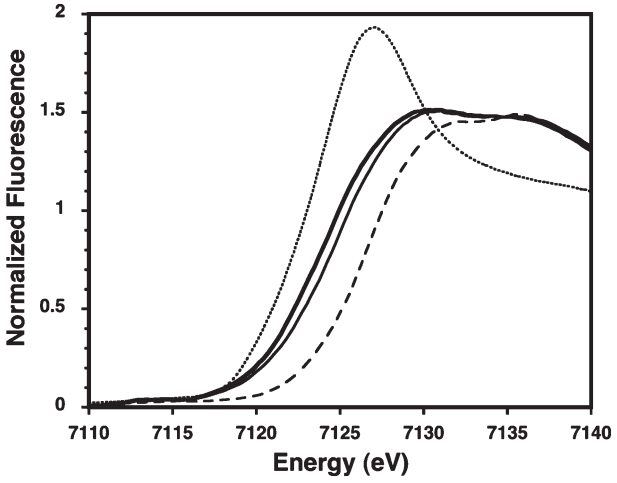

FIGURE 8: Normalized XANES spectra of iron-loaded *A. cellulolyticus* P_{1B-5}-Hr (light solid line) and azide-treated *A. cellulolyticus* P_{1B-5}-Hr (bold solid line), compared with the model control spectra for $(NH_4)_2Fe(SO_4)_2$ (dotted line) and $NH_4Fe(SO_4)_2$ (dashed line).

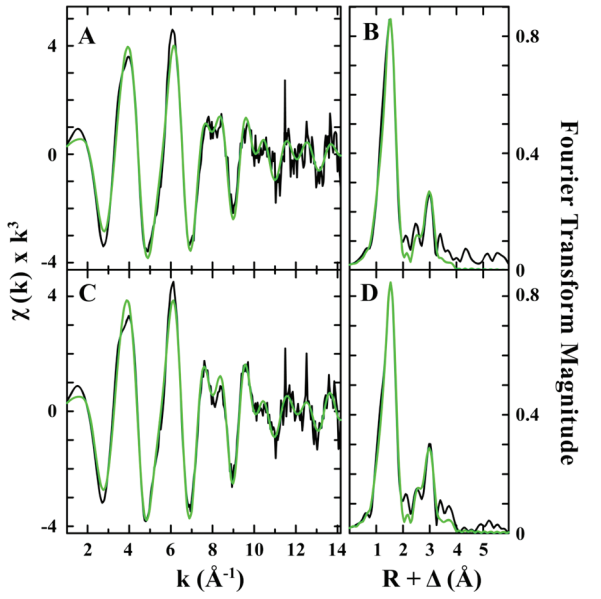

FIGURE 9: Smoothed EXAFS and Fourier transforms of EXAFS data for iron bound to iron-loaded (A and B, respectively) and azide-treated (C and D, respectively) *A. cellulolyticus* P_{1B-5}-Hr. Empirical data are shown in black, and theoretical simulations are shown in green.

latter distance is too long for a bridging oxygen atom and suggests the presence of a bridging hydroxide, as observed for the deoxy form of Hr (*52*) or, alternatively, a water molecule. The azide-treated sample is very similar to the iron-loaded sample, which is not surprising since the Fe−N distance in azide adducts of Hr is approximately 2 Å (*32*, *50*). The Fe−Fe distance is unchanged, suggesting that binding of azide does not alter the dinuclear center core structure in any appreciable manner as would be expected if azide was bridging the two metal ions. Thus, azide is likely binding in a terminal fashion, as observed for other Hr adducts. Long-range carbon scattering environments at ca. 3.0 and 4.1 Å are observed in both samples. Carbon scattering at these bond distances is typical in the presence of rigid imidazole scattering from histidine residues acting as metal ligands (*53*).

Functional Implications. The combined metal binding and spectroscopic data indicate that P_{1B-5}-Hr houses a diiron center, similar to that in other Hr proteins and domains. Hr domains have been implicated in a variety of biological functions. In invertebrates, Hr reversibly binds O_2 for transport (*54*). Prokaryotic Hr proteins and domains fall into two groups: single domain proteins or domains fused to larger proteins. Rigorous functional characterization has not been performed, but putative functions include O_2 transport (*M. capsulatus* (Bath) Hr) (*42*, *55*), O_2 sensing for chemotaxis (DcrH-Hr) (*31*), nitric oxide sensing (*56*), iron storage (*40*, *57*), and cadmium detoxification (*58*). In humans, iron sensing by the Hr domain of FBXL5 leads to degradation of iron regulatory proteins (*46*, *59*).

Soluble metal binding domains in other P_{1B}-ATPases play a regulatory role, likely via metal-dependent protein−protein interactions with other domains. For example, Cu^+ binding by the N-terminal MBDs of P_{1B-1}-ATPases precludes protein−protein interactions with the ATPBD (*60*, *61*). Although the substrate of the P_{1B-5}-ATPases has not been identified, the discovery of a soluble Hr domain provides intriguing clues. One possibility is that these ATPases transport iron. By analogy to the P_{1B-1}-ATPases, iron binding to P_{1B-5}-Hr might affect transport by modulating interdomain interactions. An alternative or additional function of P_{1B-5}-Hr might involve O_2 sensing. For DcrH-Hr, conformational changes upon O_2 binding to the diiron(II) site are proposed to initiate signal transduction that leads to anaerotaxis (*32*). For the P_{1B-5}-ATPases, sensing of O_2 as well as iron would have the added benefit of preventing oxidative damage: under oxidative stress conditions, the iron-loaded Hr domain would initiate iron efflux, minimizing the potentially damaging effects of iron-mediated Fenton chemistry.

Another possibility is that iron binding and/or O_2 sensing regulate(s) transport of another metal ion. Notably, the *A. cellulolyticus* genome encodes a nickel-containing superoxide dismutase, and O_2 sensing could play a role in its regulation by maintaining appropriate Ni^{2+} concentrations. Another potentially O_2-regulated system present in *A. cellulolyticus* is NiFe hydrogenase (*62*). This idea is consistent with the observation (vide supra) that some *Burkholderia* species encode P_{1B-5}-ATPases and cytochrome b_{561}-like proteins in the same operon, and cytochrome b_{561}-like proteins may be associated with NiFe hydrogenase (*38*, *39*). There could also be synergism or antagonism between iron and the transported metal substrate. Although testing of these hypotheses will require functional characterization of a full-length P_{1B-5}-ATPase, the identification of P_{1B-5}-Hr suggests a novel regulatory mechanism for P_{1B}-ATPases and expands the known functional repertoire of Hr domains.

ACKNOWLEDGMENT

We thank J. Argüello for valuable discussions. We also thank Dr. Chi-Hao Luan and Brendon Dusel of the High Throughput Analysis Laboratory at Northwestern University for help in collecting and analyzing thermal stability data.

SUPPORTING INFORMATION AVAILABLE

Gel filtration data for purified P_{1B-5}-Hr and a list of 195 identified P_{1B-5}-ATPase sequences. This material is available free of charge via the Internet at http://pubs.acs.org.

REFERENCES

1. Lutsenko, S., and Kaplan, J. H. (1995) Organization of P-type ATPases: significance of structural diversity. *Biochemistry 34*, 15607–15613.

2. Axelsen, K. B., and Palmgren, M. G. (1998) Evolution of substrate specificities in the P-type ATPase superfamily. *J. Mol. Evol. 46*, 84–101.
3. Rensing, C., Mitra, B., and Rosen, B. P. (1997) The *zntA* gene of *Escherichia coli* encodes a Zn(II)-translocating P-type ATPase. *Proc. Natl. Acad. Sci. U.S.A. 94*, 14326–14331.
4. Rensing, C., Sun, Y., Mitra, B., and Rosen, B. P. (1998) Pb(II)-translocating P-type ATPases. *J. Biol. Chem. 273*, 32614–32617.
5. Sharma, R., Rensing, C., Rosen, B. P., and Mitra, B. (2000) The ATP hydrolytic activity of purified ZntA, a Pb(II)/Cd(II)/Zn(II)-translocating ATPase from *Escherichia coli*. *J. Biol. Chem. 275*, 3873–3878.
6. Mana-Capelli, S., Mandal, A. K., and Argüello, J. M. (2003) *Archaeoglobus fulgidus* CopB is a thermophilic Cu^{2+}-ATPase. *J. Biol. Chem. 278*, 40534–40541.
7. Mandal, A. K., Cheung, W. D., and Argüello, J. M. (2002) Characterization of a thermophilic P-type Ag^{+}/Cu^{+}-ATPase from the extremophile *Archaeglobus fulgidus*. *J. Biol. Chem. 277*, 7201–7208.
8. Rutherford, J. C., Cavet, J. S., and Robinson, N. J. (1999) Cobalt-dependent transcriptional switching by a dual-effector MerR-like protein regulates a cobalt-exporting variant CPx-type ATPase. *J. Biol. Chem. 274*, 25827–25832.
9. Rensing, C., Ghosh, M., and Rosen, B. P. (1999) Families of soft-metal-ion-transporting ATPases. *J. Bacteriol. 181*, 5891–5897.
10. Tottey, S., Rich, P. R., Rondet, S. A., and Robinson, N. J. (2001) Two Menkes-type ATPases supply copper for photosynthesis in *Synechocystis* PCC 6803. *J. Biol. Chem. 276*, 19999–20004.
11. Bull, P. C., and Cox, D. W. (1994) Wilson disease and Menkes disease: new handles on heavy-metal transport. *Trends Genet. 10*, 246–252.
12. Williams, L. E., Pittman, J. K., and Hall, J. L. (2000) Emerging mechanisms for heavy metal transport in plants. *Biochim. Biophys. Acta 1465*, 104–126.
13. Lutsenko, S., and Petris, M. J. (2003) Function and regulation of the mammalian copper-transporting ATPases: insights from biochemical and cell biological approaches. *J. Membr. Biol. 191*, 1–12.
14. Argüello, J. M. (2003) Identification of ion-selectivity determinants in heavy-metal transport P_{1B}-type ATPases. *J. Membr. Biochem. 195*, 93–108.
15. Argüello, J. M., Eren, E., and González-Guerrero, M. (2007) The structure and function of heavy metal transport P_{1B}-type ATPases. *Biometals 20*, 233–248.
16. Mandal, A. K., and Argüello, J. M. (2003) Functional roles of metal binding domains of the *Archaeoglobus fulgidus* Cu^{+}-ATPase CopA. *Biochemistry 42*, 11040–11047.
17. Fan, B., and Rosen, B. P. (2002) Biochemical characterization of CopA, the *Escherichia coli* Cu(I)-translocating P-type ATPase. *J. Biol. Chem. 277*, 46987–46992.
18. Boal, A. K., and Rosenzweig, A. C. (2009) Structural biology of copper trafficking. *Chem. Rev. 109*, 4760–4779.
19. Eren, E., Kennedy, D. C., Maroney, M. J., and Arguello, J. M. (2006) A novel regulatory metal binding domain is present in the C terminus of *Arabidopsis* Zn^{2+}-ATPase HMA2. *J. Biol. Chem. 281*, 33881–33891.
20. Barry, A. N., Shinde, U., and Lutsenko, S. (2010) Structural organization of human Cu-transporting ATPases: learning from building blocks. *J. Biol. Inorg. Chem. 15*, 47–59.
21. Scherer, J., and Nies, D. H. (2009) CzcP is a novel efflux system contributing to transition metal resistance in *Cupriavidus metallidurans* CH34. *Mol. Microbiol. 73*, 601–621.
22. Stenkamp, R. E. (1994) Dioxygen and hemerythrin. *Chem. Rev. 94*, 715–726.
23. Altschul, S. F., Madden, T. L., Schäffer, A. A., Zhang, J., Zhang, Z., Miller, W., and Lipman, D. J. (1997) Gapped BLASTand PSI-BLAST: a new generation of protein database search programs. *Nucleic Acids Res. 25*, 3389–3402.
24. Hunter, S., Apweiler, R., Attwood, T. K., Bairoch, A., Bateman, A., Binns, D., Bork, P., Das, U., Daugherty, L., Duquenne, L., Finn, R. D., Gough, J., Haft, D., Hulo, N., Kahn, D., Kelly, E., Laugraud, A., Letunic, I., Lonsdale, D., Lopez, R., Madera, M., Maslen, J., McAnulla, C., McDowall, J., Mistry, J., Mitchell, A., Mulder, N., Natale, D., Orengo, C., Quinn, A. F., Selengut, J. D., Sigrist, C. J. A., Thimma, M., Thomas, P. D., Valentin, F., Wilson, D., Wu, C. H., and Yeats, C. (2009) InterPro: the integrative protein signature database. *Nucleic Acids Res. 37*, D211–D215.
25. Finn, R. D., Mistry, J., Tate, J., Coggill, P., Heger, A., Pollington, J. E., Gavin, O. L., Gunasekaran, P., Ceric, G., Forslund, K., Holm, L., Sonnhammer, E. L. L., Eddy, S. R., and Bateman, A. (2010) The Pfam protein families database. *Nucleic Acids Res. 38*, D211–D222.
26. Thompson, J. D., Higgins, D. G., and Gibson, T. J. (1994) CLUSTAL W: improving the sensitivity of progressive multiple sequence alignment through sequence weighting, position-specific gap penalties and weight matrix choice. *Nucleic Acids Res. 22*, 4673–4680.
27. Geourjon, C., and Deleage, G. (1995) SOPMA: significant improvements in protein secondary structure prediction by consensus prediction from multiple alignments. *Comput. Appl. Biosci. 11*, 681–684.
28. Claros, M. G., and von Heijne, G. (1994) Toppred-II—an improved software for membrane-protein structure predictions. *Comput. Appl. Biosci. 10*, 685–686.
29. Bendtsen, J. D., Nielsen, H., von Heijne, G., and Brunak, S. (2004) Improved prediction of signal peptides: SignalP 3.0. *J. Mol. Biol. 340*, 783–795.
30. Barabote, R. D., Xie, G., Leu, D. H., Normand, P., Necsulea, A., Daubin, V., Medigue, C., Adney, W. S., Xu, X. C., Lapidus, A., Parales, R. E., Detter, C., Pujic, P., Bruce, D., Lavire, C., Challacombe, J. F., Brettin, T. S., and Berry, A. M. (2009) Complete genome of the cellulolytic thermophile *Acidothermus cellulolyticus* 11B provides insights into its ecophysiological and evolutionary adaptations. *Genome Res. 19*, 1033–1043.
31. Xiong, J., Kurtz, D. M., Jr., Ai, J., and Sanders-Loehr, J. (2000) A hemerythrin-like domain in a bacterial chemotaxis protein. *Biochemistry 39*, 5117–5125.
32. Isaza, C. E., Silaghi-Dumitrescu, R., Iyer, R. B., Kurtz, D. M., Jr., and Chan, M. K. (2006) Structural basis for O_2 sensing by the hemerythrin-like domain of a bacterial chemotaxis protein: substrate tunnel and fluxional N terminus. *Biochemistry 45*, 9023–9031.
33. Lowry, O. H., Rosebrough, N. J., Farr, A. L., and Randall, R. J. (1951) Protein measurement with the Folin phenol reagent. *J. Biol. Chem. 193*, 265–275.
34. Davydov, R., Valentine, A. M., Komar-Panicucci, S., Hoffman, B. M., and Lippard, S. J. (1999) An EPR study of the dinuclear iron site in the soluble methane monooxygenase from *Methylococcus capsulatus* (Bath) reduced by one electron at 77 K: the effects of component interactions and the binding of small molecules to the diiron(III) center. *Biochemistry 38*, 4188–4197.
35. Telser, J., Davydov, R., Horng, Y. C., Ragsdale, S. W., and Hoffman, B. M. (2001) Cryoreduction of methyl-coenzyme M reductase: EPR characterization of forms, MCR_{ox1} and MCR_{red1}. *J. Am. Chem. Soc. 123*, 5853–5860.
36. Cook, J. D., Bencze, K. Z., Jankovic, A. D., Crater, A. K., Busch, C. N., Bradley, P. B., Stemmler, A. J., Spaller, M. R., and Stemmler, T. L. (2006) Monomeric yeast frataxin is an iron-binding protein. *Biochemistry 45*, 7767–7777.
37. Bencze, K. Z., Kondapalli, K. C., and Stemmler, T. L. (2007) X-ray absorption spectroscopy, in Applications of Physical Methods to Inorganic and Bioinorganic Chemistry: Handbook, Encyolopedia of Inorganic Chemistry (Scott, R. A., and Lukehart, C. M., Eds.) 2nd ed., pp 513−528, John Wiley & Sons, Chichester, U.K.
38. Gross, R., Pisa, R., Sänger, M., Lancaster, R. D., and Simon, J. (2004) Characterization of the menaquinone reduction site in the diheme cytochrome *b* membrane anchor of *Wolinella succinogenes* NiFe-hydrogenase. *J. Biol. Chem. 279*, 274–281.
39. Yoon, K.-S., Tsukada, N., Sakai, Y., Ishii, M., Igarashi, Y., and Nishihara, H. (2008) Isolationand characterization of a new facultatively autotrophic hydrogen-oxidizing Betaproteobacterium, *Hydrogenophaga* sp. AH-24. *FEMS Microbiol. Lett. 278*, 94–100.
40. French, C. E., Bell, J. M. L., and Ward, F. B. (2008) Diversity and distribution of hemerythrin-like proteins in prokaryotes. *FEMS Microbiol. Lett. 279*, 131–145.
41. Bailly, X., Vanin, S., Chabasse, C., Mizuguchi, K., and Vinogradov, S. N. (2008) A phylogenomic profile of hemerythrins, the nonheme diiron binding respiratory proteins. *BMC Evol. Biol.* 8.
42. Kao, W.-C., Wang, V. C.-C., Huang, Y.-C., Yu, S. S.-F., Chang, T.-C., and Chan, S. I. (2008) Isolation, purification, and characterization of hemerythrin from *Methylococcus capsulatus* (Bath). *J. Inorg. Biochem. 102*, 1607–1614.
43. Solomon, E. I., Brunold, T. C., Davis, M. I., Kemsley, J. N., Lee, S.-K., Lehnert, N., Neese, F., Skulan, A., Yang, Y.-S., and Zhou, J. (2000) Geometric and electronic structure/function correlations in non-heme iron enzymes. *Chem. Rev. 100*, 235–349.
44. Garbett, K., Darnall, D. W., Klotz, I. M., and Williams, R. J. (1969) Spectroscopy and structure of hemerythrin. *Arch. Biochem. Biophys. 135*, 419–434.
45. Zhang, J.-H., and Kurtz, D. M., Jr. (1991) Reconstitution of the diiron sites in hemerythrin and myohemerythrin. *Biochemistry 30*, 583–589.
46. Salahudeen, A. A., Thompson, J. W., Ruiz, J. C., Ma, H. W., Kinch, L. N., Li, Q., Grishin, N. V., and Bruick, R. K. (2009) An E3 ligase possessing an iron-responsive hemerythrin domain is a regulator of iron homeostasis. *Science 326*, 722–726.

47. Shiemke, A. K., Loehr, T. M., and Sanders-Loehr, J. (1984) Resonance Raman study of the μ-oxo-bridged binuclear iron center in oxyhemerythrin. *J. Am. Chem. Soc. 106*, 4951–4956.
48. Davydov, R., Kuprin, S., Graslund, A., and Ehrenberg, A. (1994) Electron-paramagnetic-resonance study of the mixed-valent diiron center in *Escherichia coli* ribonucleotide reductase produced by reduction of radical-free protein R2 at 77 K. *J. Am. Chem. Soc. 116*, 11120–11128.
49. DeWitt, J. G., Bentsen, J. G., Rosenzweig, A. C., Hedman, B., Green, J., Pilkington, S., Papaefthymiou, G. C., Dalton, H., Hodgson, K. O., and Lippard, S. J. (1991) X-ray absorption, Mössbauer, and EPR studies of the dinuclear iron center in the hydroxylase component of methane monooxygenase. *J. Am. Chem. Soc. 113*, 9219–9235.
50. Holmes, M. A., and Stenkamp, R. E. (1991) Structures of met and azidomet hemerythrin at 1.66 Å resolution. *J. Mol. Biol. 220*, 723–737.
51. Holmes, M. A., Trong, I. L., Turley, S., Sieker, L. C., and Stenkamp, R. E. (1991) Structures of deoxy and oxy hemerythrin at 2.0 Å resolution. *J. Mol. Biol. 218*, 583–593.
52. Zhang, K., Stern, E. A., Ellis, F., Sanders-Loehr, J., and Shiemke, A. K. (1988) The active site of hemerythrin as determined by X-ray absorption fine structure. *Biochemistry 27*, 7470–7479.
53. Stemmler, T. L., Sossong, T. M., Jr., Goldstein, J. I., Ash, D. E., Elgren, T. E., Kurtz, D. M., Jr., and Penner-Hahn, J. E. (1997) EXAFS comparison of the dimanganese core structures of manganese catalase, arginase and manganese-substituted ribonucleotide reductase and hemerythrin. *Biochemistry 36*, 9847–9858.
54. Klotz, I. M., and Kurtz, D. M. (1984) Binuclear oxygen carriers—hemerythrin. *Acc. Chem. Res. 17*, 16–22.
55. Karlsen, O. A., L., R., Bruseth, L. J., Larsen, Ø., Brenner, A., Berven, F. S., Jensen, H. B., and Lillehaug, J. R. (2005) Characterization of a prokaryotic haemerythrin from the methanotrophic bacterium *Methylococcus capsulatus* (Bath). *FEBS J. 272*, 2428–2440.
56. Strube, K., de Vries, S., and Cramm, R. (2007) Formation of a dinitrosyl iron complex by NorA, a nitric oxide-binding di-iron protein from *Ralstonia eutropha* H16. *J. Biol. Chem. 282*, 20292–20300.
57. Baert, J. L., Britel, M., Sautiere, P., and Malecha, J. (1992) Ovohemerythrin, a major 14-kDa yolk protein distinct from vitellogenin in leech. *Eur. J. Biochem. 209*, 563–569.
58. Demuynck, S., Li, K. W., Van der Schors, R., and Dhainaut-Courtois, N. (1993) Amino acid sequence of the small cadmium-binding protein (MP II) from *Nereis diversicolor* (annelida, polychaeta). Evidence for a myohemerythrin structure. *Eur. J. Biochem. 217*, 151–156.
59. Vashisht, A. A., Zumbrennen, K. B., Huang, X. H., Powers, D. N., Durazo, A., Sun, D. H., Bhaskaran, N., Persson, A., Uhlen, M., Sangfelt, O., Spruck, C., Leibold, E. A., and Wohlschlegel, J. A. (2009) Control of iron homeostasis by an iron-regulated ubiquitin ligase. *Science 326*, 718–721.
60. González-Guerrero, M., Hong, D., and Argüello, J. M. (2009) Chaperone-mediated Cu^+ delivery to Cu^+ transport ATPases. Requirement of nucleotide binding. *J. Biol. Chem. 284*, 20804–20811.
61. Tsivkovskii, R., MacArthur, B. C., and Lutsenko, S. (2001) The Lys^{1010}-Lys^{1325} fragment of the Wilson's disease protein binds nucleotides and interacts with the N-terminal domain of this protein in a copper-dependent manner. *J. Biol. Chem. 276*, 2234–2242.
62. Vignais, P. M., and Billoud, B. (2007) Occurrence, classification, and biological function of hydrogenases: an overview. *Chem. Rev. 107*, 4206–4272.